NÖHÜ Müh. Bilim. Derg. / NOHU J. Eng. Sci., Erken Görünüm / InPress

Niğde Ömer Halisdemir Üniversitesi Mühendislik Bilimleri Dergisi
Niğde Ömer Halisdemir University Journal of Engineering Sciences

Araştırma makalesi / Research article

www.dergipark.org.tr/tr/pub/ngumuh / www.dergipark.org.tr/en/pub/ngumuh

Evaluating the impact of sonication process on graphene oxide structural properties

Sonikasyon işleminin grafen oksit yapısal özellikleri üzerindeki etkisinin değerlendirilmesi

Fatih Sargin[1], Funda Ak Azem[2,*], Kursat Kanbur[3], Isil Birlik[4], Ahmet Turk[5]

[1,3] *Dokuz Eylul University, The Graduate School of Natural and Applied Sciences, Department of Metallurgical and Materials Engineering, 35160, İzmir, Türkiye*
[1,3,5] *Manisa Celal Bayar University, Department of Metallurgical and Materials Engineering, 45140, Manisa, Türkiye*
[2,4] *Dokuz Eylul University, Department of Metallurgical and Materials Engineering, 35160, İzmir, Türkiye*
[2,4] *Dokuz Eylul University, The Graduate School of Natural and Applied Sciences, Department of Nanoscience and Nanoengineering, 35160, İzmir, Türkiye*

Abstract

Graphene oxide (GO) is one of the members of carbon-based nanomaterials and can be featured as a graphene structure decorated with various oxygenated functional groups. Hummers method is one of the most known and versatile methods for the production of GO nanomaterials because of its ease of application, parameter controllability, and high yield. This process enables graphite oxidation and exfoliation into single or multi-layered GO sheets. Exfoliation separates multilayered graphite oxide flakes or particles; it forms single layer GO by forcing oxidizing agents or solvent molecules between layers. The sonication process can exfoliate the oxidized layers, resulting in the formation of GO structure when the exfoliated layers consist of only one or a few layers of carbon atoms. This process is considered among the key parameters of the Hummers method that influence the characteristics of GO-based nanomaterials. In this study, the impact of sonication process parameters, duration time, and power on morphological and structural characteristics of GO development was examined. For this purpose, characterization studies were performed by using a Scanning electron microscope (SEM), X-ray diffraction (XRD), Fourier-transform infrared spectroscopy (FTIR), UV-Vis spectroscopy, and Raman spectroscopy analysis. It has been determined that the increase in applied sonication power and duration causes the distance between layers to decrease and defects to increase in the resulting GO structure. The findings revealed that the sample treated with the lowest power and shortest sonication time had the highest interlayer distance value of 7.83Å and the lowest C/O ratio of 1.62. Consequently, it exhibited the highest oxidation level compared to the other samples.

Keywords: Graphene oxide, Exfoliation, Sonication

Öz

Karbon bazlı nanomalzemelerin üyelerinden biri olan grafen oksit (GO), basitçe çeşitli oksijen içerikli fonksiyonel gruplarca dekore edilmiş grafen yapısı olarak da tanımlanabilmektedir. Hummers yöntemi, uygulama kolaylığı, parametre kontrol edilebilirliği ve yüksek verimi nedeniyle GO nanomalzemelerinin üretimi için en sık kullanılan, çok yönlü yöntemlerden biridir. Bu yöntem, başlangıç malzemesi olan grafitin oksidasyonunu ve tek veya birkaç katmanlı GO tabakaları şeklinde katmanlara ayrılmasına imkân vermektedir. Eksfoliasyon, çok katmanlı grafit oksit tabakalarının veya parçacıklarının birbirinden ayrılması, oksitleyici ajanların veya solvent moleküllerinin bu katmanlar arasına girmesi sürecidir. Sonikasyon işlemi ise oksitlenmiş katmanları birbirinden ayırarak yalnızca bir veya birkaç karbon atomundan meydana gelen tek katmanlı GO yapısının oluşmasını sağlamaktadır. Bu proses GO bazlı nanomalzemelerin özelliklerini etkileyen Hummers yönteminin temel parametreleri arasında yer almaktadır. Bu çalışmada sonikasyon işlem süresi ve güç parametrelerinin GO nanomalzemlerin morfolojik ve yapısal özelliklerine etkisi incelenmiştir. Bu amaçla taramalı elektron mikroskobu (SEM), X-ışını kırınımı (XRD), Fourier-transform kızılötesi spektroskopisi (FTIR), UV-Vis spektroskopisi ve Raman spektroskopisi analizi kullanılarak karakterizasyon çalışmaları yapılmıştır. Uygulanan sonikasyon gücü ve süresindeki artışın katmanlar arası mesafenin azalmasına ve elde edilen GO yapısında kusurların artmasına neden olduğu tespit edilmiştir. Bulgular, en düşük güç ve en kısa sonikasyon süresine tabii tutulan numunenin, 7,83Å ile en yüksek katmanlar arası mesafe değerine ve 1,62 ile en düşük C/O oranına sahip olduğunu ortaya çıkardı. Sonuç olarak, diğer numunelerle kıyasla en yüksek oksidasyon seviyesini sergilemiştir.

Anahtar kelimeler: Grafen oksit, Eksfoliasyon, Sonikasyon

* Sorumlu yazar / Corresponding author, e-posta / e-mail: funda.ak@deu.edu.tr (F. Ak Azem)
Geliş / Recieved: 22.04.2024 Kabul / Accepted: 16.07.2024 Yayımlanma / Published: xx.xx.20xx
doi: 10.28948/ngmuh.1470478

1 Introduction

Graphene is a single-layer structure that consists of carbon atoms in the form of a honeycomb. In this structure, carbon atoms form sp2 bonds, which results in excellent mechanical, electrical, and thermal properties [1]. Despite its outstanding qualities, the main drawbacks of graphene are its limited production capacity and applicability due to its nature. GO is another member of the carbon nanomaterial family in a single-layer form. GO has been classified as one of the most prevalent highly oxidized graphene derivatives based on its microstructural properties. It has numerous oxygen functional groups and a large surface area, which makes it highly reactive [2]. GO, a derivative of graphene is a versatile material that offers a wide range of advantages and shows excellent shielding performance, high aspect ratio, ultrahigh strength, ultrahigh thermal conductivity, high surface activity, and other properties of graphene. Moreover, it features a carboxyl group, hydroxyl group, epoxy group, and other functional groups that can be used to prepare a variety of derivatives [3,4]. These functional groups make GO soluble because of the high affinity of these groups for water molecules [5,6]. Even though GO's superior properties, such as easy production, good solubility, a wide range of application areas, and ease of surface modification, are enough for its reputation, it is also known for its reduction properties, which result in the formation of reduced graphene oxide (rGO), a material that similar to graphene [7]. GO has a wide range of application areas such as electronic devices, sensors, optical materials, photovoltaic devices, energy storage devices, photocatalytic applications, batteries, supercapacitors, water and air filters, bioimaging, biosensors, drug delivery systems and scaffolds [8]. Top-down techniques are the primary methods for producing graphene from graphite. These approaches consist of solvent exfoliation or oxidation/exfoliation/reduction. Brodie, Staudenmaier, and Hummers used conventional chemical oxidation operations to prepare GO. These processes utilize graphite as the raw material for an oxidation reaction using various strong oxidants peeled off to produce GO [4,9–13].

Hummers Method is considered one of the most efficient and fast routes compared to other methods [7]. This method was initially proposed by Hummer and Offman in 1958, and the researchers have made various modifications and improvements throughout time [1,7,14–16]. The preparation approach for Hummers GO can be considered a two-step process. First, graphite is oxidized by a mixture of oxidizing and intercalating chemicals. Then, it is exfoliated in water to produce single-layered GO sheets. This process results in the production of single-layered GO sheets [17]. In the first stage, graphite combines with an acidic solution and transforms into an intercalation compound. In the second step of ongoing transformation, intercalated graphite reacts with strong oxidizing agents and forms pristine graphite oxide (PGO). Because of diffusion, PGO consists of graphitic layers with oxidizing agents between each layer. At the final stage, water enters the structure, and PGO transforms into GO by exfoliating graphitic layers [17,18].

Nowadays, researchers are aiming to produce GO faster, safer, cheaper, and more efficiently. For this purpose, the exfoliation of graphitic layers gains much importance. Since Van der Waals bonds hold graphitic layers together, a complete exfoliation is required to separate these layers and produce single-layered structures [19]. Exfoliation is simply the result of the destruction of Van der Waals bonds between graphitic layers [20]. Therefore, a weak affinity between graphitic layers is required for improved exfoliation. As graphite oxidation occurs due to the reaction between solution and graphite layers, functional groups form between graphite layers and increase the inter-layer spacing, contributing to the exfoliation [21].

Exfoliation of GO layers can be achieved by several approaches, such as chemical exfoliation [22], electrochemical exfoliation [23], thermal treatment, and liquid phase exfoliation [19]. In the liquid phase exfoliation, exfoliation can be obtained by sonication or mixing. It was noted that the characteristics of the obtained powder can be changed according to exfoliation parameters such as type of solvent, centrifugation process sonication type, and apparatus [23, 24]. In this context, the sonication process is one of the favored approaches for improving the oxidation degree and exfoliation of the final product. In the sonication process, mechanical vibrations caused by high-frequency ultrasound waves cause cavitation and create mechanical pressure waves. Depending on the parameters of the sonication process, the local high temperature produced by the cavitation phenomenon causes faster oxidation of the graphite [25]. To the best of our knowledge, studies in the literature have generally focused on optimizing sonication time using bath sonication [26–28]. The exfoliation process is relatively more effective because sonication with probe sonication significantly affects van der Walls forces in graphite materials. Based on this point, the relationship between ultrasound power and time in the sonication process performed with the probe was investigated in the study. Sabbaghan et al. showed that ultrasonic waves can produce enough energy to break down the Van der Waals bonds in the graphitic structure, which leads to the exfoliation of graphite oxide structures [29]. Botas et al. subjected GO solutions to ultrasound waves from 0.5 h to 24 h [30]. Their results showed that exfoliation yield was increased, and the lateral size of GO sheets was decreased with the increasing sonication time. Similarly, Kumar et al. investigated the effect of sonication in an ultrasonic bath with a power output of 100 W for periods between 5 and 60 min. The authors proved that with increasing sonication time, the interlayer distance of GO sheets and the O/C ratio of GO products increased [31]. In a different approach, Yang et al. used a tabletop ultrasonication cleaner to exfoliate graphite oxide to GO and produced highly oxidized GO films [32].

Herein, we propose a systematic approach to observing the effect of sonication time and power on GO production. In this context, GO solutions were sonicated by a sonication probe with varying time and power parameters. SEM (Energy-dispersive X-ray spectroscopy), EDX, XRD, FTIR, Raman, and UV- Vis analysis were performed to evaluate the structural properties and oxidation degree of resultant GO products.

2 Material and methods

2.1 Materials

Graphite powder (with a powder size of 20 µm), sulphuric acid (H_2SO_4, 95%-98% purity), phosphoric acid (H_3PO_4, 85%), potassium permanganate ($KMnO_4$, 99%), hydrogen peroxide (H_2O_2, 30%), hydrochloric acid (HCl, 37%) were purchased from Sigma Aldrich (St. Louis, MO).

2.2 GO production

GO samples have been developed using the Modified Hummers technique. Graphite powder was added to H_2SO_4/H_3PO_4 (v/v%) solution and stirred in an ice bath for one h. Then, $KMnO_4$ was added to the mixture. Afterward, 100 mL of deionized water was gradually added to the mixture. Mechanical stirring was kept for 1 hour after the water addition was completed. Finally, the solution was boosted with deionized water and H_2O_2. After adding H_2O_2 to the solution, the color of the solution changed from black to dark brown. The resultant solution was centrifuged to remove excess water, and GO slurry was obtained. To remove retained ions and other residues, GO slurry was washed with HCl solution and deionized water several times until a neutral pH was obtained. Following the washing step, the resultant GO solution was exfoliated using sonication. A schematic flow chart of GO production is demonstrated in Figure 1. The effect of exfoliation was controlled by the sonication process, which involved varying time and power outputs. The sonication process was done by Bandelin Sonopulse HD2200, an ultrasonic homogenizer. Table 1 displays the abbreviations for the produced GO samples under various sonication conditions. After the sonication process, the GO solutions were dried overnight in atmospheric conditions. Figure 2 shows the obtained GO sample after the drying process.

Table 1. Abbreviations of the produced GO samples

Samples	Sonication Time (min)	Sonication Power (Watt)
S1	10	30
S2	20	30
S3	10	50
S4	20	50

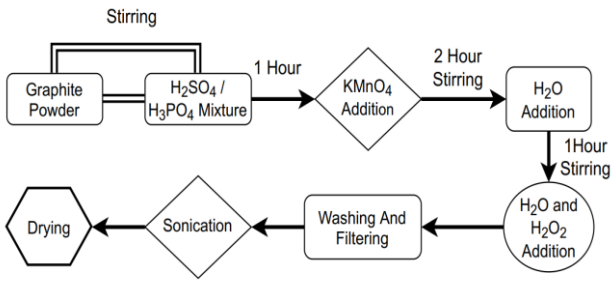

Figure 1. Schematic flow chart of GO production

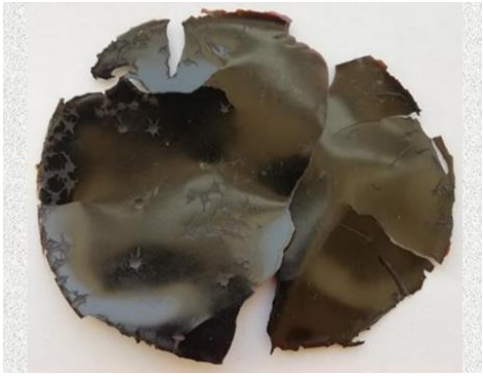

Figure 2. S1 sample was obtained after the drying step

2.3 Materials characterization

X-ray diffraction (XRD) analysis was performed using a Rigaku DMax-2100/PC X-ray diffractometer with Cu-Kα radiation to evaluate the phase structure and oxidation degree of each synthesized GO sample as well as graphite powder for comparison. SEM equipped with EDX was used to investigate the morphology and evaluate the chemical composition of each GO sample (Zeiss Gemini SEM 500). FTIR spectroscopy of samples was performed with a Thermo Scientific FTIR Spectrometer with an ATR module in the range of 500-4000 cm^{-1} wavenumbers to determine the functional groups in GO structure. Furthermore, UV-visible spectra of samples were taken with a Thermo Scientific Evolution 260 BIO UV spectrometer for 200-600 nm wavelength. A Renishaw Raman Spectrometer with a 532 nm laser source was used to investigate Raman spectroscopy investigation in the 230-3200 cm^{-1} wavenumber region.

3 Results and discussions

X-ray diffraction patterns of graphite powder and produced GO samples are given in Figure 3. XRD pattern of graphite consisted of a main peak with a high intensity at 2θ of about 26°, which corresponded to the (002) plane (JCPDS No: 41-1487) [33]. Additionally, the XRD pattern of GO samples exhibits a characteristic main peak at approximately 11° (2θ) corresponding to the (001) plane as identified by JCPDS card No: 00-065-1528 [34]. It was reported that GO nanomaterials exhibit a main peak between 9-12° depending on their production method and oxidation degree. The peak location (001) enables a comparison of the interlayer distance in all examined samples [35, 36]. The difference in XRD patterns between graphite and produced GO can be seen clearly, as the main peak of samples shifted to smaller 2θ angles. The 2θ shifts occurring in GO structures can be interpreted depending on the production mechanism. During GO production, an acid mixture first penetrates between graphite layers. Then, the oxidizing agent diffuses to graphite interlayers, which eventually results in the oxidation of graphite and the formation of various functional groups [18]. As oxidation occurs, more functional groups are introduced between layers, which expands interlayer distance [37]. Using Bragg's law, interlayer distances between derived GO samples were calculated from XRD data. Table 2 shows the interlayer spacing (d_{002}) and crystallite size values for all samples calculated using

Bragg's law and the Scherrer equation, respectively [36]. As can be seen, graphite had a lower interlayer distance value than GO samples since it had high crystallinity and a well-ordered structure. Furthermore, oxidation during the modified Hummers method resulted in greater interlayer distance values for GO samples. The S1 sample with a main peak of 11.34° (2θ) had the highest interlayer distance value of 7.83Å, which indicated its high oxidation degree. Moreover, the S4 sample had the lowest interlayer distance value of 7.52Å. In this context, an increase in the interlayer distance of GO nanomaterials means an increase in the oxidation degree. Chen et al. demonstrated that mechanical exfoliation of GO sheets can be achieved through sonication [4]. The interplanar distance can be used to interpret the degree of oxidation or the number of functional groups attached to the basal plane of GO, which increases with higher oxidation levels [38]. Thus, this result could be attributed to obtained GO nanomaterials with the highest interlayer distance value, which tend to be better oxidized and well exfoliated. Additionally, results indicated that the (002) peak shifts toward a lower 2θ value, which suggests an increase in the interlayer d-spacing. With the increasing number of oxygen-related functional groups bonded to the carbon basal plane with Van der Waals, interlayer distance and oxidation degree could be increased. However, the fragile nature of Van der Waals bonding also bears the possibility of removal of such functional groups [16]. Furthermore, the intensity of the (001) peak in the X-ray diffraction pattern of GO is employed to assess the oxidation degree [38]. Sample S1 shows a more intense (001) peak, suggesting higher oxidation levels than other samples. It has been observed that as the ultrasonic power increases, the degradation effect of ultrasonics increases, resulting in the loss of functional groups and decreasing interlayer spacing. Although the exfoliation process generally increases interlayer distance and takes place during sonication, it was reported that excessive usage of sonication may destroy GO layers and reduce functional groups [5, 30]. Mellado et al. applied different sonication times to GO samples and found that the XRD peak position and oxidation degree of sonicated samples altered with the applied procedure. The authors additionally reported that GO sheets were fragmented and experienced structural damage due to intense sonication [5]. On the other hand, Sabbaghan et al. proved that it was possible to remove the functional groups of GO structure and produce reduced GO nanomaterials with the help of an appropriate sonication procedure. Consequently, the interlayer distance decreases with increasing sonication time and power due to excessive sonication [29]. Also, secondary peaks around 21.23° and 26° in S2 and S3 samples might indicate the removal of functional groups and the reduction of GO samples in small quantities [39-41]. Furthermore, crystallite size calculations showed that crystallite size remarkably decreased with the oxidation of graphite. The S4 sample, which has a crystallite size value of 2.32 nm, is shown to have the lowest value of all the synthesized GO samples (Table 2). It was understood that the sonication process led to breaking GO sheets into smaller fragments. The reason behind the GO sheets separating into small fragments was identified as the sonication method [5]. Kumar et al. interpreted that the reduction in crystallite size is associated with the reduction in GO domains due to oxidation-induced structural disorder in the form of sp3 hybridized carbon atoms [42].

Therefore, as the sonication power output increases, the samples experience excessive GO layer exfoliation, reducing the crystallite size and the interlayer spacing. On the other hand, the intensity of the (001) peak in sample S3 decreased, indicating a lower oxidation level than other samples. According to the literature, some studies showed that, in some cases, decreasing oxidation degree and exfoliation rate affects crystallite size inversely [43, 44]. The result obtained regarding the crystallite size determined for sample S3 is compatible with the literature. In this context, the increase in crystallite size in sample S3, which has a lower oxidation level, is interpreted as the presence of relatively more damaged functional group bonds rather than C=C bonds [45].

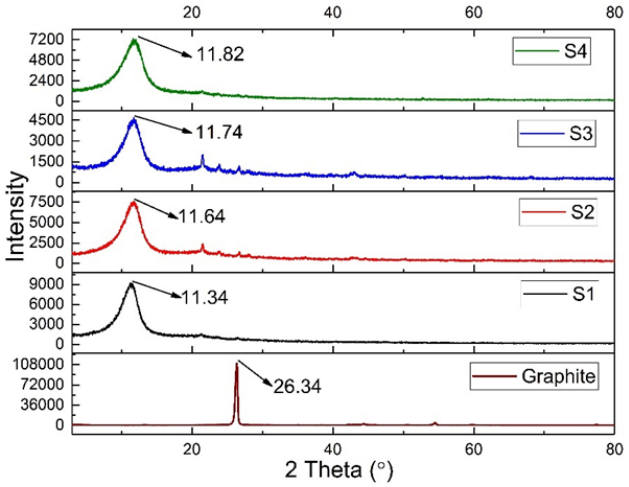

Figure 3. XRD spectra of graphite and GO samples

Table 2. Interlayer spacing (d_{002}) and crystallite size values of graphite and GO samples

Sample	Graphite	S1	S2	S3	S4
Interlayer spacing (Å)	3.47	7.83	7.63	7.57	7.52
Crystallite size (nm)	22.26	2.7	2.67	2.85	2.32

FTIR spectroscopy was performed to identify the functional groups present in the GO samples. The GO structure has a variety of oxygen functional groups, such as carbonyl (C=O), carboxyl (-COOH), hydroxyl (-OH), and epoxy (C-O-C) [36, 43]. The FTIR spectra of GO samples produced with different sonication parameters are given in Figure 4. Also, the FTIR spectrum of graphite powder is provided in the same figure for a better evaluation of functional group formation. The broad peak around 3200-3500 cm^{-1} was attributed to O-H vibrations of adsorbed water trapped in the GO structure [37].

Another characteristic GO peak around 1720 cm^{-1} was attributed to carboxyl vibrations. The presence of the absorption peak at 1610 cm^{-1} can be assigned to sp2

hybridized C=C bonds [36, 44]. In addition, absorption peaks around 1228, 1048, and 972 cm^{-1} indicate the presence of epoxy, alkoxy C-O stretching, and C-O bending vibrations, respectively [43, 45]. According to Figure 4, all the samples have characteristic GO functional groups in their structure. The presence of functional groups that contain oxygen confirms that the graphite has successfully oxidized into GO [46].

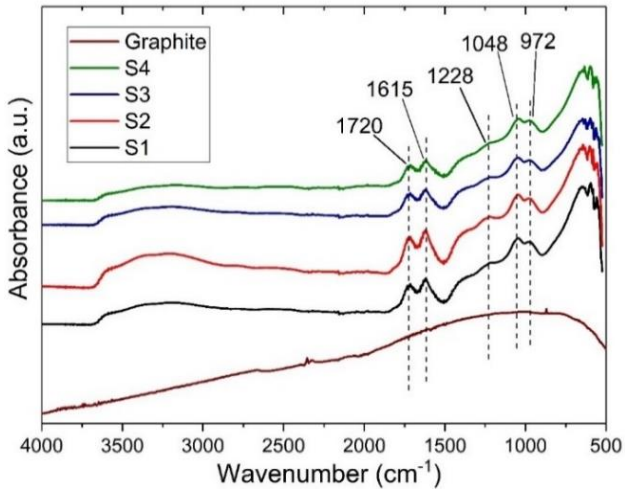

Figure 4. FTIR spectra of graphite and synthesized GO samples

On the other hand, the low absorption degree of peaks around 3200 cm^{-1} indicates that S3 and S4 samples had relatively less O-H bonds in their structure [14]. Therefore, S1 and S2 samples might have slightly more functional groups in their structure compared to S3 and S4 [35]. It is seen that the intensity of the peaks for the oxygen-containing functional groups decreases with higher sonication time and power. Yoo and Park produced GO nanomaterials with different oxidation degrees. Their FTIR analysis proved that with the decrease in oxidation degrees, some functional groups vanished or diminished from the spectra [35]. It is seen that the intensity of the functional groups decreases in GO structures obtained through different sonication parameters [47].

Figure 5 depicts the UV-Vis absorption spectra of GO samples with different sonication parameters. According to the literature, characteristic UV-Vis spectra of GO nanomaterials show a strong absorption peak at 230 nm, which corresponds π-π* transitions of C=C bonding, and a slight shoulder around 300 nm, which corresponds to n- π* transitions C=O bonds [36, 37]. It was seen that all samples had similar carbon rings in their basal plane, and the change of sonication parameters had not caused a significant change in sp2 conjugated carbon formation [14]. Adjusting the amount of oxygen-containing functional groups can significantly alter the optical properties of GO. Figure 4 showed that all samples proved to have GO characteristic π-π* and n- π* transitions, which agreed with FTIR results in the literature [35].

Studies showed that GO nanomaterials show p-type semiconductor behavior thanks to their oxygen-containing functional groups [48]. The band gap energy of GO nanomaterials was calculated from optical absorption spectra using Tauc's relation as given in Equation (1) [49]. The band gap energy can be derived from the intersection of a line, which is drawn from the linear region of the curve and obtained by Tauc's relation [50].

$$(\alpha h\nu)^{1/\gamma} = A\,(h\nu - Eg) \quad (1)$$

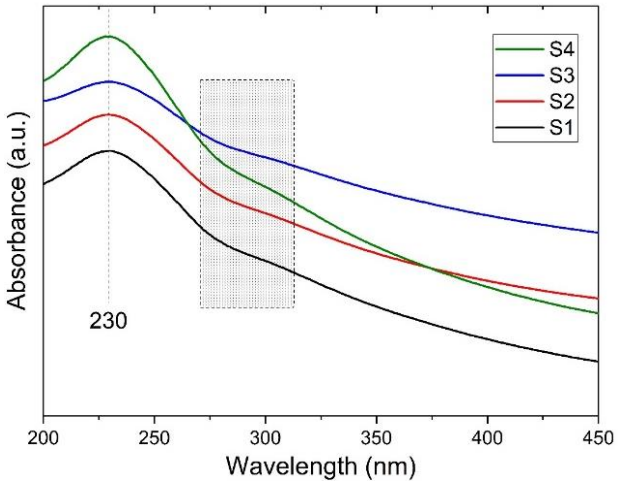

Figure 5. UV-Vis absorption spectra of GO samples

Our measurements obtained band gap values of 4.14, 4.21, 4.07, and 4.15 eV for S1, S2, S3, and S4 samples, respectively (Figure 6). According to the literature, the band gap value of GO nanoparticles can range from 2.5 to 6.5 eV [48,49]. The band gap energy of GO nanomaterials is considerably related to the number of sp2 and sp3 hybridized regions in the basal plane and holes and carbon vacancies [49,51]. Sharma et al. evaluated the optical and electrical properties of GO and rGO samples by Tauc plots. They found that rGO samples had lower band gap values than fully oxidized GO samples [52]. Also, studies revealed that an increase in the degree of reduction of GO samples gave rise to a decrease in the band gap values of rGO samples [49,53]. Although several studies showed that GO nanomaterials with higher oxidation degrees tend to have higher band gap values, detailed analysis showed that oxidation degree alone could not explain the increase or decrease in the band gap value obtained from Tauc's plots [51,54]. However, de Lima et al. proved that GO samples with comparable oxidation levels could have various band gap values. It has been interpreted that this difference is due to several reasons, such as the distribution of defects on the basal plane, distribution of sp2 hybridized carbon regions, relative area of each sp2 hybridized carbon region, amount and type of defects (holes, carbon vacancies, etc.) in the basal plane [51]. In other respects, a few studies pointed out that increasing crystallite size may decrease band gap value [55, 56]. Thus, as mentioned above, relatively higher destruction of functional group bonds rather than C=C bonds in the S3 sample may generate a low band gap value.

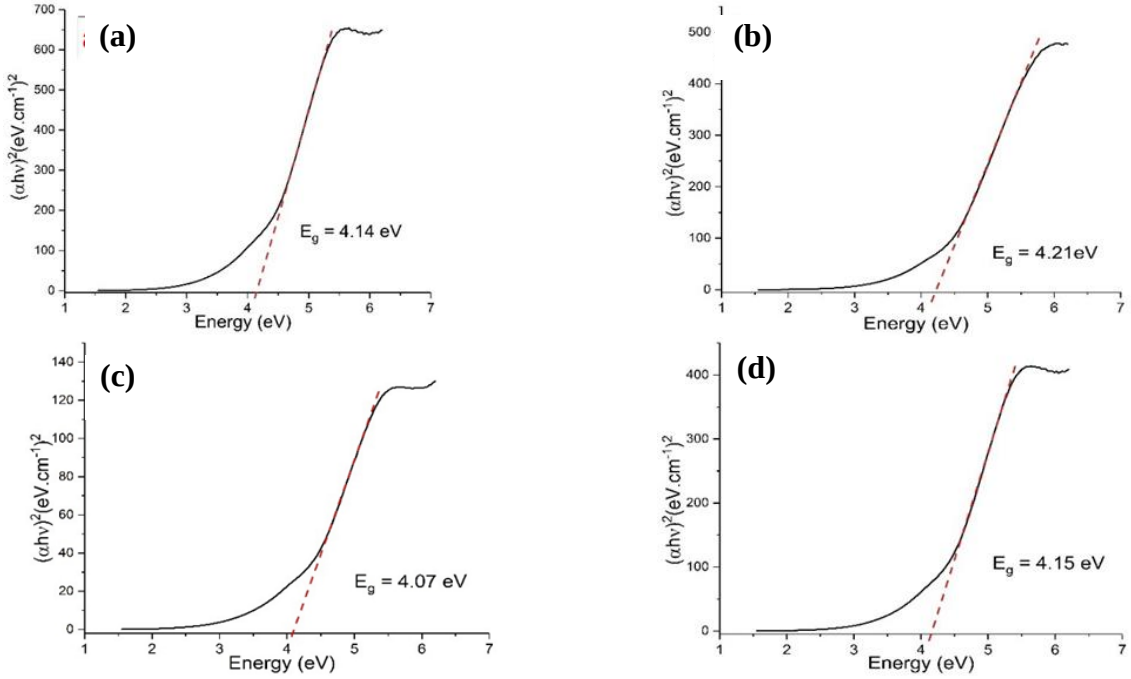

Figure 6. The optical band gap energy of GO samples (a) S1, (b) S2, (c) S3, and (d) S4

In this context, in our study, it was seen that different sonication parameters not only altered the interlayer different sonication parameters not only altered the interlayer distance and oxidation degree but also introduced defects that could change the band gap energy of each sample.

The structural characteristics of graphene oxide can be revealed by Raman spectroscopy. Figure 7 depicts Raman spectra of synthesized GO samples. Raman spectra of GO nanomaterials generally consist of two strong peaks. The G band results from the bond stretching of carbon sp2 atoms, whereas the D band is ascribed to structural instability [57]. The peak around 1355 cm^{-1}, which is known as the D band

shows defects in the carbon basal plane, such as vacancies and disorders caused by functional groups attached to carbon atoms [53,58]. The D band also shows the existence of sp3 hybridized carbon atoms accordingly [42]. On the other hand, the peak around 1590 cm^{-1}, known as the G band, originates from E2g phonon modes of graphitic structure and shows the presence of sp2 hybridized carbon atoms [42,48]. Figure 7 shows the Raman spectrum of S1, S2, S3, and S4 samples. All samples showed D and G bands around 1355 and 1590 cm^{-1}, characteristic of GO nanomaterials [59]. Studies revealed that comparing the D and G bands might be used to assess the degree of oxidation as well as the ratio of defects [42,60]. The ID/IG ratio of every sample was determined using Raman spectra. The comparable values of the S1, S2, and S3 samples were determined to be around 0.84; however, the ratio of the S4 sample was found to be 0.95. Although an increased oxidation rate is expected to increase the ID/IG ratio, it can also increase defects and functional groups. In some scenarios, Eigler and Hirsch proved that the ID/IG ratio was not constantly associated with the oxidation degree and defect ratio [61]. Therefore, Sieradzka et al. produced GO nanomaterials with various oxidation degrees and applied a reduction process to these samples. Their results showed that the ID/IG ratio of GO samples changed regardless of the oxidation degree of the samples [62]. Also, it was found that an increase in the ID/IG ratio was seen in all samples after the reduction process. Similarly, Krishnamoorthy et al. produced GO nanomaterials with different oxidation degrees. They revealed that the ID/IG ratio increased with the increasing oxidation degree up to a certain point, then decreased [63]. Other studies also reported related findings about the effect of oxidation degree and defect ratio on the ID/IG ratio of GO nanomaterials [58,64]. Information regarding the structural disorder is provided by the intensity ratio (ID/IG) of these bands; a higher ID/IG value indicates a more severe structural disorder [65]. Based on this point, even if the XRD analysis shows that the S1 sample has the highest oxidation degree, it can be interpreted that the S1 sample has fewer defects than the S4 sample. Moreover, this determination revealed that the relatively strong sonication process could lead to more structural defects than oxidative defects, especially for the S4 sample.

SEM images and EDX results of GO samples produced with varying sonication parameters are given in Figure 8. As can be seen in Figure 8, all samples showed similar morphological formations with a homogenous wrinkled surface. Produced GO samples were exfoliated and fragmented during the sonication process [5]. Because of their functional groups, GO sheets provide a homogenous colloidal solution as they were in solution. As the water evaporates throughout the drying process, the GO sheets begin to collapse on each other and over one another. After drying, the GO sheets form a layered structure resembling a film [40].

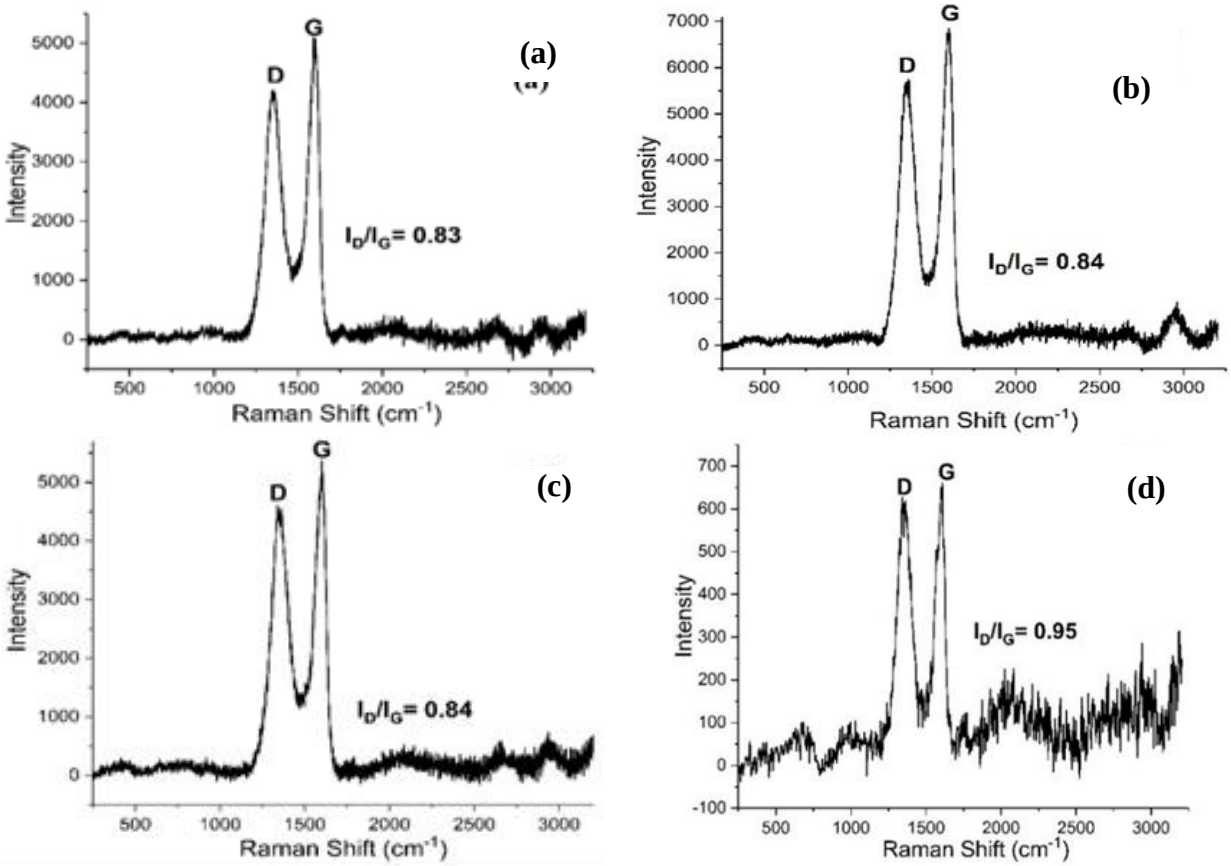

Figure 7. Raman spectra of synthesized GO samples (a) S1, (b) S2, (c) S3, and (d) S4

As mentioned in the XRD analysis, power output during the sonication led to the loss of functional groups and a decrease in interlayer distance. The observed result suggests that our sonication method was more than enough for exfoliation. Therefore, obtaining GO films after the drying procedure was quite reasonable because of our production method. Furthermore, the EDX technique was used to conduct a semi-quantitative assessment of elemental C in derivatized GO samples. EDX results in Figure 7 revealed that the samples contained no substances other than C and O, which are the main components of GO since its structure is mainly composed of C atoms arranged in a honeycomb formation and oxygenated functional groups attached to them [7].

As the EDX analysis proved that there were no contaminations or residues in the structure, it also helps to evaluate the oxidation degree of samples. The C/O ratios for samples S1, S2, S3, and S4 were calculated using the EDX data and were found to be 1.62, 1.64, 2.05, and 2.09, respectively. It can be seen that sample S1 has the lowest C/O ratio (1.69), while sample S4 has the highest ratio with a value of 2.09. Studies in the literature point out the oxidation degree of GO samples improves while the C/O ratio decreases [66,67]. EDX results demonstrate that sample S1 has a higher degree of oxidation than other samples.

The results of the characterization studies have proven that the applied sonication parameters affect the oxidation of GO samples. Although all samples had similar morphological properties and functional groups, they had different C/O ratios and interlayer spacing values. As a function of the sonication time and power throughout the sonication process, the increase in the interlayer space identified is interpreted as an increased exfoliation of the flakes, depending on the XRD patterns.

Since ultrasonic probes produce sonication regions under the contact area of the probe, ultrasonic effects produced by these devices tend to be more intense and powerful [68]. There are several drawbacks of the excessive sonication process on GO solutions reported in the literature, such as loss of functional groups, damage to sheet formation, and more wrinkled surfaces [5,26,62]. Additionally, because of the high energy output caused by the sonication probe, even C-C/C=C bonds could break, which could bring about either the formation of new oxygen groups or the folding of graphene sheets [69]. Consequently, increasing time and sonication power in our study led to highly exfoliated and less oxidized GO samples. On the other hand, it was understood that excessive sonication not only exfoliated the GO sheets but also damaged Van der Waals bonds, eventually leading to loss of oxygen related functional groups and causing an increase in C/O ratio consistent with the previous studies [5,68]. As a result, the S1 sample that was sonicated with 10 minutes and 30 W power exhibited the highest degree of oxidation, homogeneous phase development, and exfoliated structure.

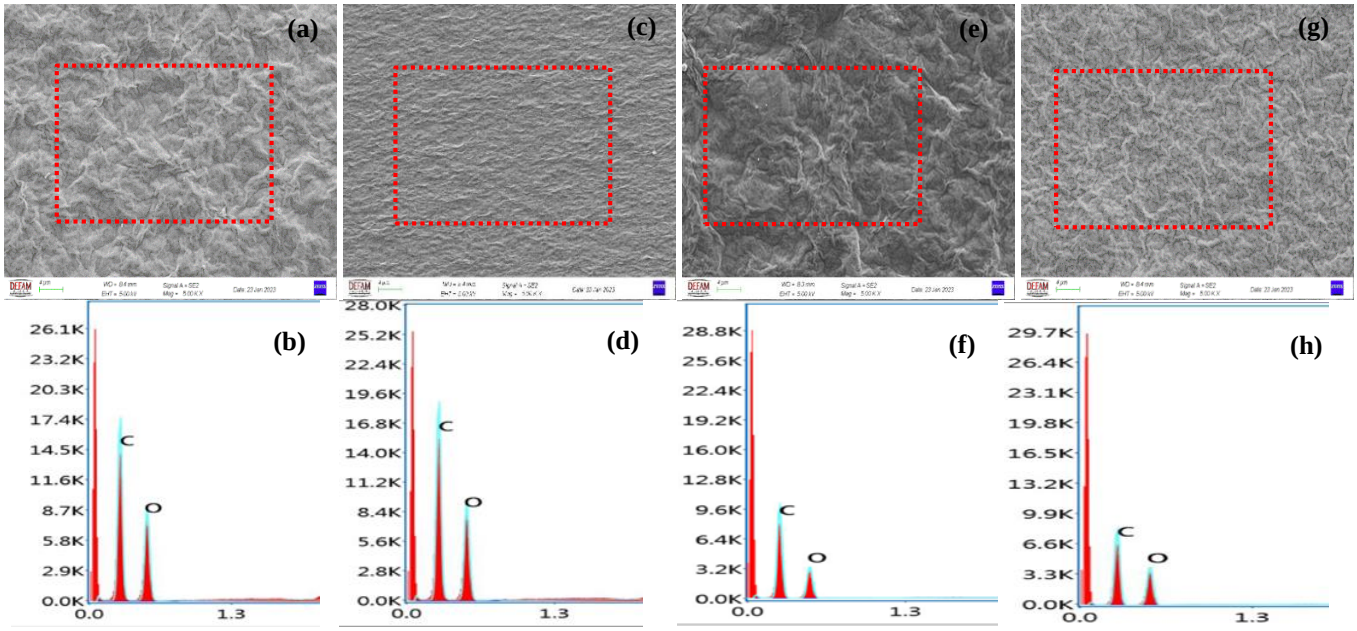

Figure 8. SEM images and EDX analyses results of GO samples (a-b) S1, (c-d) S2, (e-f) S3, and (g-h) S4

4 Conclusions

In the present study, we demonstrated the effect of the sonication process parameters on the structural properties of GO nanomaterials synthesized by the Improved Hummers method. XRD analysis results indicated the formation of GO structure and showed that increasing sonication time and power led to excessive exfoliation, decreased interlayer distance between GO sheets, and crystallite size. While FTIR analysis showed that all samples proved to have characteristic functional groups in GO structure, UV-Vis analysis showed no significant distinction among samples. Additionally, band gap calculations from optical absorption spectra revealed the highest value obtained from the S2 sample with 4.21 eV. On the other hand, Raman analysis showed that an increase in sonication power and time induced an increase in the defect ratio of GO samples. SEM results showed that with the effect of the sonication process, exfoliation and fragmentation of GO sheets occurred in all of the samples, which effectuate similar morphological properties after the drying process.

Consequently, it was demonstrated that the degree of oxidation was decreased by increasing the sonication time and power parameters investigated in the present study. Sonication power and time increased the defect ratio of GO samples. SEM results showed that with the effect of the sonication process, exfoliation and fragmentation of GO sheets occurred in all of the samples, which effectuate similar morphological properties after the drying process. Our research findings show that increasing both sonication power and time leads to decreased oxidation levels. Consequently, the S1 sample was found to have the highest oxidation level and the lowest defect rate compared to the other samples.

Acknowledgment

The authors are grateful to thank Dokuz Eylul University (DEU) Department of Metallurgical and Materials Engineering and Center for Fabrication and Application of Electronic Materials for their invaluable assistance. The authors would also like to acknowledge the Manisa Celal Bayar University Scientific Research Projects Coordination Unit (Project number: 2020-038) for their financial support of this study.

Conflict of interest

The authors declare that there is no conflict of interest.

Similarity rate (iThenticate): %14

References

[1] M. Sohail, M. Saleem, S. Ullah, N. Saeed, A. Afridi, M. Khan, and M. Arif, Modified and improved Hummer's synthesis of graphene oxide for capacitors applications. Modern Electronic Materials, 3, 110–116, 2017. https://doi.org/10.1016/j.moem.2017.07.002.

[2] A. Anwar, T.P. Chang, and C.T. Chen, Graphene oxide synthesis using a top–down approach and discrete characterization techniques: a holistic review. Carbon Letters, 32, 1–38, 2022. https://doi.org/10.1007/S42823-021-00272-Z.

[3] M.F.R. Hanifah, J. Jaafar, M.H.D. Othman, A.F. Ismail, M.A. Rahman, N. Yusof, W.N.W. Salleh, and F. Aziz, Facile synthesis of highly favorable graphene oxide: Effect of oxidation degree on the structural, morphological, thermal and electrochemical properties. Materialia, 6, 100344, 2019. https://doi.org/10.1016/j.mtla.2019.100344.

[4] X. Chen, Z. Qu, Z. Liu, and G. Ren, Mechanism of Oxidization of Graphite to Graphene Oxide by the

Hummers Method. ACS Omega, 7, 23503–23510, 2022. https://doi.org/10.1021/acsomega.2c01963.

[5] C. Mellado, T. Figueroa, R. Baez, M. Meléndrez, and K. Fernández, Effects of probe and bath ultrasonic treatments on graphene oxide structure. Materials Today Chemistry, 13, 1–7, 2019. https://doi.org/10.1016/j.mtchem.2019.04.006.

[6] P. Majumder, and R. Gangopadhyay, Evolution of graphene oxide (GO)-based nanohybrid materials with diverse compositions: an overview. RSC Advances, 12, 5686–5719, 2022. https://doi.org/10.1039/D1RA06731A.

[7] L. Sun, Structure and synthesis of graphene oxide. Chinese Journal of Chemical Engineering, 27, 2251–2260, 2019. https://doi.org/10.1016/j.cjche.2019.05.003.

[8] J. Zhao, L. Liu, and F. Li, Fabrication and Reduction. In: Graphene Oxide: Physics and Applications. Springer Briefs in Physics, Springer, Berlin, Heidelberg, 2015. https://doi.org/10.1007/978-3-662-44829-8_1.

[9] R. Ikram, B.M. Jan, and W. Ahmad, An overview of industrial scalable production of graphene oxide and analytical approaches for synthesis and characterization. Journal of Materials Research and Technology, 9, 11587–11610, 2020. https://doi.org/10.1016/J.JMRT.2020.08.050.

[10] S. Pei, Q. Wei, K. Huang, H.M. Cheng, and W. Ren, Green synthesis of graphene oxide by seconds timescale water electrolytic oxidation. Nature Communications, 9, 1–9, 2018. https://doi.org/10.1038/s41467-017-02479-z.

[11] P. Yu, Z. Tian, S.E. Lowe, J. Song, Z. Ma, X. Wang, Z.J. Han, Q. Bao, G.P. Simon, D. Li, and Y.L. Zhong, Mechanically-assisted electrochemical production of graphene oxide. Chemistry of Materials, 28, 8429–8438, 2016. https://doi.org/10.1021/acs.chemmater.6b04415.

[12] A. Poniatowska, M. Trzaskowski, and T. Ciach, Production and properties of top-down and bottom-up graphene oxide. Colloids and Surfaces A: Physicochemical and Engineering Aspects, 561, 315–324, 2019. https://doi.org/10.1016/j.colsurfa.2018.10.049.

[13] N. Kumar, R. Salehiyan, V. Chauke, O. Joseph Botlhoko, K. Setshedi, M. Scriba, M. Masukume, and S. Sinha Ray, Top-down synthesis of graphene: A comprehensive review. FlatChem, 27, 100224, 2021. https://doi.org/10.1016/J.FLATC.2021.100224.

[14] D.C. Marcano, D. V. Kosynkin, J.M. Berlin, A. Sinitskii, Z. Sun, A. Slesarev, L.B. Alemany, W. Lu, and J.M. Tour, Improved synthesis of graphene oxide. ACS Nano, 4, 4806–4814, 2010. https://doi.org/10.1021/nn1006368.

[15] A.A. Olorunkosebi, M.A. Eleruja, A.V. Adedeji, B. Olofinjana, O. Fasakin, E. Omotoso, K.O. Oyedotun, E.O.B. Ajayi, and N. Manyala, Optimization of graphene oxide through various Hummers' methods and comparative reduction using green approach. Diamond and Related Materials, 117, 108456, 2021. https://doi.org/10.1016/J.DIAMOND.2021.108456.

[16] N.I. Zaaba, K.L. Foo, U. Hashim, S.J. Tan, W.W. Liu, and C.H. Voon, Synthesis of Graphene Oxide using Modified Hummers Method: Solvent Influence. Procedia Engineering, 184, 469-477, 2017. https://doi.org/10.1016/j.proeng.2017.04.118.

[17] J. Liu, S. Chen, Y. Liu, and B. Zhao, Progress in preparation, characterization, surface functional modification of graphene oxide: A review. Journal of Saudi Chemical Society, 26, 2022. https://doi.org/10.1016/J.JSCS.2022.101560.

[18] A.M. Dimiev, and J.M. Tour, Mechanism of graphene oxide formation. ACS Nano, 8, 3060–3068, 2014. https://doi.org/10.1021/nn500606a.

[19] M. Cai, D. Thorpe, D.H. Adamson, and H.C. Schniepp, Methods of graphite exfoliation. Journal of Materials Chemistry, 22, 24992–25002, 2012. https://doi.org/10.1039/c2jm34517j.

[20] N. Liu, Q. Tang, B. Huang, and Y. Wang, Graphene Synthesis: Method, Exfoliation Mechanism and Large-Scale Production. Crystals, 12, 25, 12, 25, 2021. https://doi.org/10.3390/CRYST12010025.

[21] R. Yuan, J. Yuan, Y. Wu, L. Chen, H. Zhou, and J. Chen, Efficient synthesis of graphene oxide and the mechanisms of oxidation and exfoliation. Applied Surface Science, 416, 868–877, 2017. https://doi.org/10.1016/j.apsusc.2017.04.181.

[22] L.M. Viculis, J.J. Mack, O.M. Mayer, H.T. Hahn, and R.B. Kaner, Intercalation and exfoliation routes to graphite nanoplatelets. Journal of Materials Chemistry, 15, 974–978, 2005. https://doi.org/10.1039/B413029D.

[23] C.-Y. Su, A.-Y. Lu, Y. Xu, F.-R. Chen, A.N. Khlobystov, and L.-J. Li, High-Quality Thin Graphene Films from Fast Electrochemical Exfoliation. ACS Nano, 5, 2332–2339, 2011. https://doi.org/10.1021/nn200025p.

[24] Y. Xu, H. Cao, Y. Xue, B. Li, and W. Cai, Liquid-Phase Exfoliation of Graphene: An Overview on Exfoliation Media, Techniques, and Challenges. Nanomaterials, 8, 942, 2018. https://doi.org/10.3390/NANO8110942.

[25] K. Muthoosamy, and S. Manickam, State of the art and recent advances in the ultrasound-assisted synthesis, exfoliation and functionalization of graphene derivatives. Ultrasonics Sonochemistry, 39, 478–493, 2017. https://doi.org/10.1016/J.ULTSONCH.2017.05.019.

[26] Y. Arao, and M. Kubouchi, High-rate production of few-layer graphene by high-power probe sonication. Carbon, 95, 802–808, 2015. https://doi.org/10.1016/J.CARBON.2015.08.108.

[27] A. Ručigaj, J.G. Connell, M. Dular, and B. Genorio, Influence of the ultrasound cavitation intensity on reduced graphene oxide functionalization. Ultrasonics Sonochemistry, 90, 106212, 2022. https://doi.org/10.1016/J.ULTSONCH.2022.106212.

[28] G.T.T. Le, N. Chanlek, J. Manyam, P. Opaprakasit, N. Grisdanurak, and P. Sreearunothai, Insight into the ultrasonication of graphene oxide with strong changes

in its properties and performance for adsorption applications. Chemical Engineering Journal, 373, 1212–1222, 2019. https://doi.org/10.1016/J.CEJ.2019.05.108.

[29] M. Sabbaghan, H. Charkhan, M. Ghalkhani, and J. Beheshtian, Ultrasonic route synthesis, characterization and electrochemical study of graphene oxide and reduced graphene oxide. Research on Chemical Intermediates, 45, 487–505, 2019. https://doi.org/10.1007/s11164-018-3613-8.

[30] C. Botas, A.M. Pérez-Mas, P. Álvarez, R. Santamaría, M. Granda, C. Blanco, and R. Menéndez, Optimization of the size and yield of graphene oxide sheets in the exfoliation step. Carbon, 63, 576–578, 2013. https://doi.org/10.1016/j.carbon.2013.06.096.

[31] S. Kumar, A. Garg, and A. Chowdhuri, Sonication effect on graphene oxide (GO) membranes for water purification applications. Materials Research Express, 6, 085620, 2019. https://doi.org/10.1088/2053-1591/ab1ffd.

[32] H. Yang, H. Li, J. Zhai, L. Sun, and H. Yu, Simple synthesis of graphene oxide using ultrasonic cleaner from expanded graphite. Industrial and Engineering Chemistry Research, 53, 17878–17883, 2014. https://doi.org/10.1021/ie503586v.

[33] S. Kumar, A.K. Ojha, B. Ahmed, A. Kumar, J. Das, and A. Materny, Tunable (violet to green) emission by high-yield graphene quantum dots and exploiting its unique properties towards sun-light-driven photocatalysis and supercapacitor electrode materials. Materials Today Communications, 11, 76–86, 2017. https://doi.org/10.1016/J.MTCOMM.2017.02.009.

[34] R. Al-Gaashani, Y. Zakaria, O.S. Lee, J. Ponraj, V. Kochkodan, and M.A. Atieh, Effects of preparation temperature on production of graphene oxide by novel chemical processing. Ceramics International, 47, 10113–10122, 2021. https://doi.org/10.1016/J.CERAMINT.2020.12.159.

[35] M.J. Yoo, and H.B. Park, Effect of hydrogen peroxide on properties of graphene oxide in Hummers method. Carbon, 141, 515–522, 2019. https://doi.org/10.1016/j.carbon.2018.10.009.

[36] D.G. Trikkaliotis, A.C. Mitropoulos, and G.Z. Kyzas, Low-cost route for top-down synthesis of over- and low-oxidized graphene oxide. Colloids and Surfaces A: Physicochemical and Engineering Aspects, 600, 124928, 2020. https://doi.org/10.1016/j.colsurfa.2020.124928.

[37] N. Yadav, and B. Lochab, A comparative study of graphene oxide: Hummers, intermediate and improved method. FlatChem, 13, 40–49, 2019. https://doi.org/10.1016/j.flatc.2019.02.001.

[38] S. Zainab, S. Fraz, S.U. Awan, D. Hussain, S. Rizwan, and W. Mehmood, Optimized time dependent exfoliation of graphite for fabrication of Graphene/GO/GrO nanocomposite based pseudo-supercapacitor. Scientific Reports 13, 1–16, 2023. https://doi.org/10.1038/s41598-023-41309-9.

[39] M.P. Lavin-Lopez, J.L. Valverde, L. Sanchez-Silva, and A. Romero, Solvent-Based Exfoliation via Sonication of Graphitic Materials for Graphene Manufacture. Industrial and Engineering Chemistry Research, 55, 845–855, 2016. https://doi.org/10.1021/ACS.IECR.5B03502.

[40] D. Konios, M.M. Stylianakis, E. Stratakis, and E. Kymakis, Dispersion behaviour of graphene oxide and reduced graphene oxide. Journal of Colloid and Interface Science, 430, 108–112, 2014. https://doi.org/10.1016/j.jcis.2014.05.033.

[41] S. Thakur, and N. Karak, Green reduction of graphene oxide by aqueous phytoextracts. Carbon, 50, 5331–5339, 2012. https://doi.org/10.1016/j.carbon.2012.07.023.

[42] N. Kumar, and V.C. Srivastava, Simple Synthesis of Large Graphene Oxide Sheets via Electrochemical Method Coupled with Oxidation Process. ACS Omega, 3, 10233–10242, 2018. https://doi.org/10.1021/acsomega.8b01283.

[43] J. Guerrero-Contreras, and F. Caballero-Briones, Graphene oxide powders with different oxidation degree, prepared by synthesis variations of the Hummers method. Materials Chemistry and Physics, 153, 209–220, 2015. https://doi.org/10.1016/J.MATCHEMPHYS.2015.01.005.

[44] G.Q. Qi, J. Cao, R.Y. Bao, Z.Y. Liu, W. Yang, B.H. Xie, and M.B. Yang, Tuning the structure of graphene oxide and the properties of poly(vinyl alcohol)/graphene oxide nanocomposites by ultrasonication. Journal of Materials Chemistry A, 1, 3163–3170, 2013. https://doi.org/10.1039/C3TA01360J.

[45] Z. Baig, O. Mamat, M. Mustapha, A. Mumtaz, K.S. Munir, and M. Sarfraz, Investigation of tip sonication effects on structural quality of graphene nanoplatelets (GNPs) for superior solvent dispersion. Ultrasonics Sonochemistry, 45, 133–149, 2018. https://doi.org/10.1016/J.ULTSONCH.2018.03.007.

[46] M.F.R. Hanifah, J. Jaafar, M. Aziz, A.F. Ismail, M.A. Rahman, and M.H.D. Othman, Synthesis of Graphene Oxide Nanosheets via Modified Hummersâ€™ Method and Its Physicochemical Properties. Jurnal Teknologi, 74, 195–198, 2015. https://doi.org/10.11113/JT.V74.3555.

[47] T. Soltani, and B. Kyu Lee, A benign ultrasonic route to reduced graphene oxide from pristine graphite. Journal of Colloid and Interface Science, 486, 337–343, 2017. https://doi.org/10.1016/J.JCIS.2016.09.075.

[48] D.T. Phan, and G.S. Chung, P–n junction characteristics of graphene oxide and reduced graphene oxide on n-type Si(111). Journal of Physics and Chemistry of Solids, 74, 1509–1514, 2013. https://doi.org/10.1016/J.JPCS.2013.02.007.

[49] A. Mathkar, D. Tozier, P. Cox, P. Ong, C. Galande, K. Balakrishnan, A. Leela Mohana Reddy, and P.M. Ajayan, Controlled, Stepwise Reduction and Band Gap Manipulation of Graphene Oxide. The Journal of

Physical Chemistry Letters, 3, 986–991, 2012. https://doi.org/10.1021/jz300096t.
[50] P. Makuła, M. Pacia, and W. Macyk, How To Correctly Determine the Band Gap Energy of Modified Semiconductor Photocatalysts Based on UV-Vis Spectra. Journal of Physical Chemistry Letters, 9, 6814–6817, 2018. https://doi.org/10.1021/acs.jpclett.8b02892
[51] A.H. de Lima, C.T. Tavares, C.C.S. da Cunha, N.C. Vicentini, G.R. Carvalho, B. Fragneaud, I.O. Maciel, C. Legnani, W.G. Quirino, L.F.C. de Oliveira, F. Sato, and J.P.A. de Mendonça, Origin of optical bandgap fluctuations in graphene oxide. The European Physical Journal B, 93, 1–12, 2020. https://doi.org/10.1140/EPJB/E2020-100578-7
[52] N. Sharma, S. Tomar, M. Shkir, R. Kant Choubey, and A. Singh, Study of Optical and Electrical Properties of Graphene Oxide. Materials Today: Proceedings, 36, 730–735, 2021. https://doi.org/10.1016/J.MATPR.2020.04.861.
[53] P. Gangwar, S. Singh, and N. Khare, Study of optical properties of graphene oxide and its derivatives using spectroscopic ellipsometry. Applied Physics A: Materials Science and Processing, 124, 1–8, 2018. https://doi.org/10.1007/S00339-018-1999-1.
[54] K.O. Olumurewa, B. Olofinjana, O. Fasakin, M.A. Eleruja, E.O.B. Ajayi, K.O. Olumurewa, B. Olofinjana, O. Fasakin, M.A. Eleruja, and E.O.B. Ajayi, Characterization of High Yield Graphene Oxide Synthesized by Simplified Hummers Method. Graphene, 6, 85–98, 2017. https://doi.org/10.4236/GRAPHENE.2017.64007.
[55] Fauzia, M.A. Khan, M. Chaman, and A. Azam, Antibacterial and sunlight-driven photocatalytic activity of graphene oxide conjugated CeO2 nanoparticles. Scientific Reports, 14, 1–17, 2024. https://doi.org/10.1038/s41598-024-54905-0.
[56] C. Aydin, H. Aydin, M. Taskin, and F. Yakuphanoglu, A Novel Study: The Effect of Graphene Oxide on the Morphology, Crystal Structure, Optical and Electrical Properties of Lanthanum Ferrite Based Nano Electroceramics Synthesized by Hydrothermal Method. Journal of Nanoscience and Nanotechnology, 19, 2547–2555, 2018. https://doi.org/10.1166/JNN.2019.15841.
[57] A.C. Ferrari, Raman spectroscopy of graphene and graphite: Disorder, electron–phonon coupling, doping and nonadiabatic effects. Solid State Communications, 143, 47–57, 2007. https://doi.org/10.1016/J.SSC.2007.03.052.
[58] M. PriyaDarshani, and R. Sharma, Controlling the bandgap of graphene oxide via varying KMnO4. Optical Materials, 147, 114634, 2024. https://doi.org/10.1016/J.OPTMAT.2023.114634.
[59] K. Haubner, J. Murawski, P. Olk, L.M. Eng, C. Ziegler, B. Adolphi, and E. Jaehne, The Route to Functional Graphene Oxide. ChemPhysChem, 11, 2131–2139, 2010. https://doi.org/10.1002/CPHC.201000132.
[60] S. Claramunt, A. Varea, D. López-Díaz, M.M. Velázquez, A. Cornet, and A. Cirera, The importance of interbands on the interpretation of the raman spectrum of graphene oxide. Journal of Physical Chemistry C, 119, 10123–10129, 2015. https://doi.org/10.1021/ACS.JPCC.5B01590.
[61] S. Eigler, and A. Hirsch, Chemistry with Graphene and Graphene Oxide—Challenges for Synthetic Chemists. Angewandte Chemie International Edition, 53, 7720–7738, 2014. https://doi.org/10.1002/ANIE.201402780
[62] M. Sieradzka, C. Ślusarczyk, W. Biniaś, and R. Fryczkowski, The Role of the Oxidation and Reduction Parameters on the Properties of the Reduced Graphene Oxide. Coatings, 11, 166, 2021. https://doi.org/10.3390/COATINGS11020166
[63] K. Krishnamoorthy, M. Veerapandian, K. Yun, and S.J. Kim, The chemical and structural analysis of graphene oxide with different degrees of oxidation. Carbon, 53, 38–49, 2013. https://doi.org/10.1016/j.carbon.2012.10.013.
[64] A.I. Abd-Elhamid, H.F. Aly, H.A.M. Soliman, and A.A. El-Shanshory, Graphene oxide: Follow the oxidation mechanism and its application in water treatment. Journal of Molecular Liquids, 265, 226–237, 2018. https://doi.org/10.1016/J.MOLLIQ.2018.05.127.
[65] Q. Guo, S. Chen, and X. Qin, ZnO–SnO2/graphene composites as high capacity anode materials for lithium ion batteries. Materials Letters, 128, 50–53, 2014. https://doi.org/10.1016/j.matlet.2014.04.096
[66] R. Muzyka, M. Kwoka, Ł. Smędowski, N. Díez, and G. Gryglewicz, Oxidation of graphite by different modified Hummers methods. New Carbon Materials, 32, 15–20, 2017. https://doi.org/10.1016/S1872-5805(17)60102-1.
[67] Y. Hou, S. Lv, L. Liu, and X. Liu, High-quality preparation of graphene oxide via the Hummers' method: Understanding the roles of the intercalator, oxidant, and graphite particle size. Ceramics International, 46, 2392–2402, 2020. https://doi.org/10.1016/j.ceramint.2019.09.231.
[68] A. Asadi, F. Pourfattah, I. Miklós Szilágyi, M. Afrand, G. Żyła, H. Seon Ahn, S. Wongwises, H. Minh Nguyen, A. Arabkoohsar, and O. Mahian, Effect of sonication characteristics on stability, thermophysical properties, and heat transfer of nanofluids: A comprehensive review. Ultrasonics Sonochemistry, 58, 104701, 2019. https://doi.org/10.1016/J.ULTSONCH.2019.104701.
[69] S. An, Graphene Oxides in Water: Characterization, Reactivity, and Application. PhD Thesis, McKelvey School of Engineering, USA, 2018. https://doi.org/https://doi.org/10.7936/qgbq-fy39.